frontiers | Frontiers in Earth Science

TYPE Original Research
PUBLISHED 12 October 2023
DOI 10.3389/feart.2023.1268810

Check for updates

OPEN ACCESS

EDITED BY
Tianshou Ma,
Southwest Petroleum University, China

REVIEWED BY
Petr Konečný,
VSB-Technical University of Ostrava, Czechia
Zhanping Song,
Xi'an University of Architecture and Technology, China

*CORRESPONDENCE
Bing Li,
libing_libing_2007@163.com

RECEIVED 28 July 2023
ACCEPTED 28 September 2023
PUBLISHED 12 October 2023

CITATION
Liu R, Zhang L, Li H and Li B (2023), Study on the mechanical properties and energy dissipation characteristics of concrete subjected to high strain rate and sulfate attack.
Front. Earth Sci. 11:1268810.
doi: 10.3389/feart.2023.1268810

COPYRIGHT
© 2023 Liu, Zhang, Li and Li. This is an open-access article distributed under the terms of the Creative Commons Attribution License (CC BY). The use, distribution or reproduction in other forums is permitted, provided the original author(s) and the copyright owner(s) are credited and that the original publication in this journal is cited, in accordance with accepted academic practice. No use, distribution or reproduction is permitted which does not comply with these terms.

Study on the mechanical properties and energy dissipation characteristics of concrete subjected to high strain rate and sulfate attack

Ruixue Liu[1], Lianying Zhang[1], Hailong Li[2] and Bing Li[1]*

[1]School of Civil Engineering, Xuzhou University of Technology, Xuzhou, Jiangsu, China, [2]School of Science, Shandong Jianzhu University, Jinan, Shandong, China

Marine structures, such as cross-sea bridges, port constructions, and offshore drilling platforms, are not only subjected to sulfate erosion, but also to various dynamic loads. Analyzing the damage evolution process of concrete under sulfate erosion and impact loads is the key to improving the lifespan of concrete. In order to study the damage evolution process of eroded concrete under high strain rates, the energy dissipation characteristics, basic physics and mechanical properties, and micro-fracture mechanism of sulfate-eroded concrete at different sulfate concentrations (C=0, 3%, 6%, and 9%) under high strain rate ranging from 70/s to 85/s are systematically studied by using the split Hopkinson pressure bar (SHPB) test system, X-ray diffractometer and SEM scanning electron microscope. The research results indicate that an increase in sulfate concentration leads to a decrease in $Ca(OH)_2$ content and an increase in Ettringite (AFt) content in concrete specimens; As the sulfate concentration increases, the dynamic peak strength and dynamic elastic modulus of concrete specimens gradually decrease, while the dynamic peak strain of concrete specimens gradually increases; The degree of macroscopic fragmentation in concrete specimens subjected to impact compression becomes increasingly severe with rising sulfate concentrations; As the sulfate concentration increases, the proportion of reflected energy and dissipated energy gradually increases, while that of transmitted energy gradually decreases, and the energy absorption capacity of the sample is significantly improved; The results of the SEM test shows that with the increase of sulfate concentration, a large amount of AFt is generated at the joint fissures and the interface of cement aggregates, the expansion of AFt and the crack development of concrete reduce the integrity and stability of concrete. This study holds significant guidance for the application of concrete in impact situations under a sulfate attack environment.

KEYWORDS

concrete, sulfate attack, strain rate, dynamic mechanical properties, energy dissipation characteristics, micromorphology

1 Introduction

With the growing number of marine structures, such as cross-sea bridges, port constructions, and offshore drilling platforms, the utilization of marine concrete is progressively increasing. Due to prolonged exposure of concrete to seawater, the presence of sulfate abundant in seawater leads to severe erosion of the concrete (Santhanam and Otieno, 2016; QiangEnvelopeZw et al., 2022). In addition, sulfates are more commonly present in subsoil and wastewater. At the same time, concrete has been frequently used high strain rate environments such as vehicle load, wind load, earthquake action and waves, and the concrete is more easily destroyed after sulfate attack in this environment. Therefore, studying the impact of sulfate attack on the mechanical properties and energy dissipation of concrete under high strain rates has strong engineering significance for the concrete application under the sulfate attack environments.

The existing research on concrete subjected to the sulfate attack has shown that sulfates induce physical and chemical reactions in concrete (Li et al., 2020), which significantly affects the stability (HUANGFU et al., 2004), durability (Xu et al., 2012), strength (Yao and Li, 2018; Peng et al., 2019), pore structure (LiShiLi et al., 2019; ChenLiuYu, 2020), and other properties of concrete. Tai I. et al. (Tai et al., 2016) discussed the expansion and cracking of concrete structures caused by sulfate attack. Considering the mechanical effect of sulfate attack on concrete, Cefis N. et al. (Cef and isComi, 2014) proposed a biphasic chemical elastic damage model. Yao J. et al. (YaoChen, 2022) found that ion erosion in the ocean leads to corrosion degradation of concrete materials, and this phenomenon causes the gradual decline of macroscopic physical and mechanical properties of concrete with the erosion time. Chen Chaohui et al. (Chen et al., 2008) conducted uniaxial compression tests on sulfate-corroded concrete. The results showed that after erosion, the elastic modulus, compressive strength, and residual deformation capacity of the concrete decrease, and the more severe the erosion, the more severe the peeling phenomenon of the concrete specimen during the loading process, and the faster the development of the main crack in the concrete. Zhu Lanfang (Zhu and Cao, 2008; Zhu, 2009) conducted a detailed study on the mechanical properties of concrete flexural members under sulfate attack. It is concluded that the cracking load value and ultimate bearing capacity of the concrete specimen decrease with the increase of sulfate concentration under long-term erosion. A series of studies have shown that sulfate has a significant impact on the physical and mechanical properties of concrete.

In recent years, concrete has gradually been utilized in environments with sulfate attack and high strain rates, and the research on the dynamic performance of concrete under sulfate attack has been highlighted (Feng et al., 2009; Xia et al., 2021; Yao et al., 2021; Bai et al., 2022; Guo et al., 2023; Wei et al., 2023). Li R. et al. (LiHouHu and Zou, 2021) observed that the elevated sulfate concentrations lead to increased mechanical damage of concrete under varying high water pressures and sulfate attack. Demei et al. (Demei et al., 2016) explored the flexural strength of concrete subjected to erosion by sulfate compounds and observed that the strength exhibited an earlier decline under dynamic load compared to static load. Liu T. et al. (Liu et al., 2012) reported that sulfate attack makes concrete strength more sensitive to strain rate, while the destructive expansion and chemical degradation caused by sulfate attack greatly reduce peak strain. Liu P. et al. (Liu et al., 2020) found that with the increase of sulfate solution concentration, the dynamic elastic modulus of concrete first increases and then decreases.

At present, research on the damage and failure laws of eroded concrete under impact load is mainly focused on the macroscopic mechanical properties. In fact, the process of damage and destruction is a process of energy dissipation. During the impact process, eroded concrete undergoes irreversible energy dissipation (Cheng et al., 2020a; Cheng et al., 2020b), which is the driving force of failure and can comprehensively reflect the internal damage and failure situation. Currently, there is limited research on the energy dissipation of eroded concrete under impact loads. Therefore, this paper conducts research on the energy dissipation and macroscopic and microscopic mechanical properties of sulfate eroded concrete under impact load, obtaining the correlation between sulfate attack concentration and energy dissipation characteristics, as well as dynamic mechanical properties and the damage evolution law of concrete is systematically studied. The research results can provide important reference for the establishment of damage evolution models and dynamic response calculations.

2 Specimen preparation and test methods

2.1 Specimen preparation

The concrete specimens were prepared in accordance with the relevant provisions of the Code for construction of concrete structures. The strength of concrete specimens was prepared in accordance with C60, and the continuous particle size of crushed stone was 5–8 mm. The concrete specimen was prepared as follows. As shown in Tables 1, 2, the cement, coarse aggregate (stone) and fine aggregate (sand) were put into the mixer and mixed for about 1 min, the water was poured into the mixer and mixed for 2 min, and then the water reducer was added and mixed for 1 min. The mixed concrete was put into a cube mold with a size of 100 × 100 × 100 mm and vibrated on the vibrating table, the surface of the specimen was smoothed and placed indoors at a room temperature; after 24 h, the specimen was demoulded. The demoulded specimen was put into the standard curing room for 28 d. The cylindrical specimen with a size of Φ74*37 mm and the non-parallelism of the two ends within 0.02 mm was processed, as shown in Figure 1.

In order to make the reflection time of the stress wave between the two ends of the sample short enough, so that the stress (strain) in the sample is quickly in a uniform state along the axis of the sample, the length of the sample should not be too large. In addition, the sample should not be too short. When the length of the sample is too short, the friction of the sample end face is relatively significant. Due to the constraint effect, an apparent strength increase will be generated, which will affect the accuracy of the experimental data. Li Xibing et al. conducted SHPB experimental research on a large number of rock and

TABLE 1 Mix ratio parameters of concrete specimens.

Water-cement ratio	Water/kgm^{-3}	Cement/kgm^{-3}	Standard sand/kgm^{-3}	Crushed stone/kgm^{-3}
0.32	145	453	740	1112

TABLE 2 Chemical composition of cement.

SiO_2 (%)	Al_2O_3 (%)	Fe_2O_3 (%)	CaO (%)	MgO (%)	Na_2O (%)	K_2O (%)	SO_3 (%)	Burning loss (%)
21.6	4.13	4.57	64.44	1.06	0.11	0.56	1.74	0.76

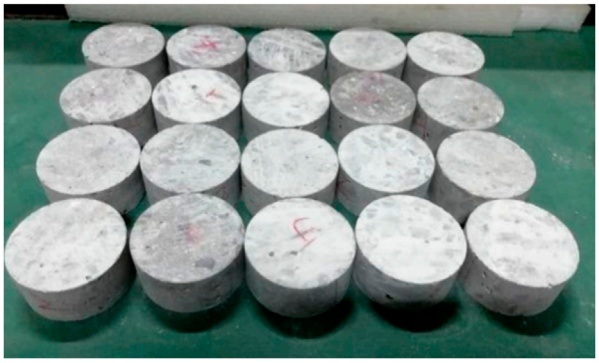

FIGURE 1
Concrete specimens.

FIGURE 2
Sulfate attack experiment.

concrete materials (Lok et al., 2001), and concluded that the inertia effect can be better eliminated when the length-diameter ratio is 0.5. Therefore, the length-diameter ratio of the sample in the impact compression experiment was set at 0.5, that is, the length of the sample was 37 mm.

Then Na_2SO_4 solutions with concentrations of 0, 3%, 6%, and 9% were prepared. The concrete specimens were put into Na_2SO_4 solutions with different concentrations, and the erosion time of

TABLE 3 Variation of mass percent w_m of calcium hydroxide, ettringite and gypsum in specimens with the corrosive solution concentration *C*.

Products	w_m/%			
	C=0.0%	*C*=3.0%	*C*=6.0%	*C*=9.0%
$Ca(OH)_2$	10.2	2.8	2.6	1.3
Ettringite (AFt)	0.4	4.9	6.5	8.3
Gypsum ($CaSO_4{\cdot}2H_2O$)	0.6	1.9	2.2	1.0

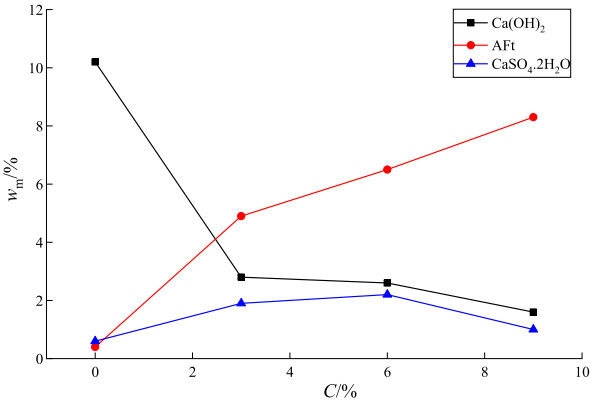

FIGURE 3
Variation of mass percent w_m of calcium hydroxide, ettringite and gypsum of concrete specimens with corrosive solution concentration *C*.

the concrete specimens was guaranteed to be 270 d after they were completely immersed in the solution. Figure 2 shows the erosion process of concrete specimens.

After the sulfate attack test was completed, the components of the concrete specimen were tested using an X-ray diffractometer (D8 ADVANCE) manufactured by Bruker Corporation. First, a drilling powder extractor was used to obtain the powder at a depth of 5 mm of the concrete specimen subjected to sulfate attack, the powder was ground to a particle size of less than 44 microns using an agate mortar, and 1 g of the powder of the concrete specimen was taken as the specimen to be measured. Second, the specimen was uniformly placed in the specimen rack and compacted by the glass plate. Third, the specimen was put into the specimen table of the X-ray diffractometer, then the

TABLE 4 Physical and mechanical parameters of concrete specimens under different sulfate concentrations and high strain rates.

C/%	Specimen number	$\dot{\varepsilon}/s^{-1}$		σ_c/MPa		E/GPa		ε_c	
		Single specimen	Average	Single specimen	Average	Single specimen	Average	Single specimen	Average
0.0	1	78.27	75.49	100.64	94.36	36.60	35.10	0.005224	0.004543
	2	73.36		87.66		33.32		0.004331	
	3	74.85		94.78		35.37		0.004073	
3.0	4	70.05	72.37	63.26	63.67	24.61	27.52	0.004211	0.004579
	5	73.06		56.38		29.88		0.004508	
	6	74.01		71.36		28.07		0.005019	
6.0	7	82.75	84.49	64.42	59.83	20.92	17.65	0.004721	0.005350
	8	84.24		58.69		13.82		0.004881	
	9	86.48		56.38		18.22		0.006447	
9.0	10	76.05	79.53	43.71	46.34	15.66	15.85	0.005680	0.006179
	11	79.78		43.52		14.69		0.007218	
	12	82.75		51.78		17.20		0.005639	

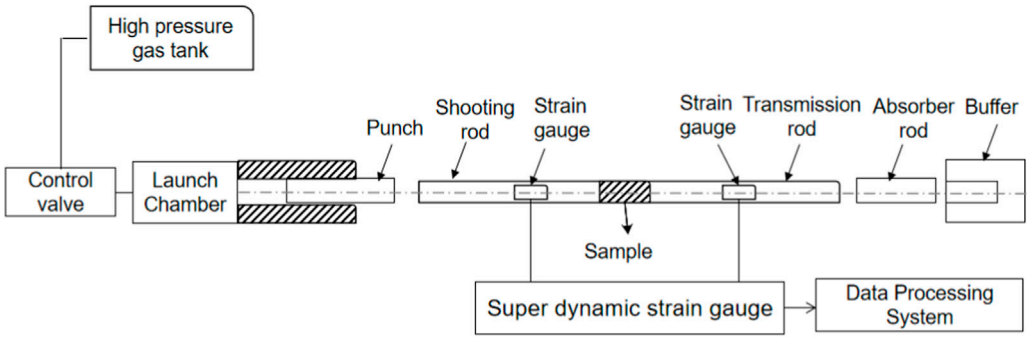

FIGURE 4
Schematic diagram of the SHPB testing system.

main power supply of the diffractometer, the switch of the circulating water system, and the power supply of the X-ray tube were turned on successively; the tube voltage and tube current was increased to the required value, diffraction parameters were set in the application software, and then the test was initiated. After the test was completed, the data were saved and analyzed. Table 3 shows the test results of different specimens.

Figure 3 shows the variation curve of mass percent w_m of the calcium hydroxide, ettringite and gypsum with the corrosive solution concentration C. As shown in Table 4 and Figure 3, the content of calcium hydroxide, AFt and gypsum in concrete has been changed following an increase in sulfate concentration. With the increase of sulfate concentration, the content of calcium hydroxide exhibits an overall downward trend, the content of AFt exhibits an overall upward trend, while the content of gypsum first increases and then decreases.

2.2 Impact test methods

The impact load test in this study was conducted by the split Hopkinson pressure bar (SHPB) test system of the State Key Laboratory for Geomechanics and Deep Underground Engineering of China University of Mining and Technology. Figure 4 shows the schematic diagram of the SHPB test system. The test system comprises of five components: a loading drive system, a pressure bar system, an energy absorption system, a signal acquisition system, and a signal processing system.

As shown in Figure 5, the specimen was placed in the SHPB test system and subject to an impact test under a pressure of about 0.5 MPa. The impact process was carried out by the following steps. 1) A certain amount of Vaseline was evenly smeared on the two end faces of the specimen, the specimen was tightly placed between the incident rod and the transmission rod,

FIGURE 5
Components of the SHPB testing system.

and the outer protective sleeve was placed on the specimen. 2) The analysis and testing system and related software were initiated, and the test parameters were set according to the experimental requirements; 3) The control valve of the air tank was opened, the inflation switch of the pressure gauge was pressed; when the pointer of the Barometer reached 0.5 MPa, the control valve of the air tank was closed, the control valve of the launching chamber was opened, the system automatically deflated, and the impact process was automatically completed. The incident wave, reflected wave and transmitted wave on the transmission rod were transmitted to the signal acquisition system through the strain gauge on the rod.

Figure 6A shows the signal obtained from the uniaxial impact compression test on concrete specimens under sulfate attack. Figure 6B tests the stress balance of the specimen. It can be seen from Figure 6B that the incident wave and reflected wave superimposed basically coincide with the transmitted wave, indicating that the assumption of stress uniformity is met.

3 Effect of erosion solution concentration on mechanical properties of concrete specimens under high strain rates

3.1 Processing methods of original data of concrete specimens

Based on the assumption of one-dimensional propagation of stress waves, the expressions of average strain $\varepsilon(t)$, average strain rate $\dot{\varepsilon}(t)$ and average stress $\sigma(t)$ of specimen materials are derived, which is the three-wave function obtained from the technical data of the SHPB test 1) (Yin et al., 2019; Lu et al., 2019):

$$\begin{cases} \varepsilon(t) = \dfrac{C_0}{L_s}\displaystyle\int_0^t [\varepsilon_I(t) - \varepsilon_R(t) - \varepsilon_T(t)]dt \\ \dot{\varepsilon}(t) = \dfrac{C_0}{L_s}[\varepsilon_I(t) - \varepsilon_R(t) - \varepsilon_T(t)] \\ \sigma(t) = \dfrac{A_0}{2A_s}E_0[\varepsilon_I(t) + \varepsilon_R(t) + \varepsilon_T(t)] \end{cases} \quad (1)$$

where $\varepsilon_I(t)$, $\varepsilon_R(t)$, and $\varepsilon_T(t)$ are strain signals of the incident wave, reflected wave, and transmitted wave; $\dot{\varepsilon}$ is the strain rate of specimen materials, s-1; $\sigma(t)$ is the average stress of specimen materials, Pa; C_0 is the longitudinal wave velocity in the pressure piece, m/s; L_S is the height of the specimen, m m; A_0 is the cross-sectional area of the compression rod, m^2; A_S is the cross-sectional area of the specimen, m^2; E_0 is the elastic modulus of the compression rod material, Pa.

According to the assumption of stress homogenization, the strain relationship between the incident rod and the transmission rod can be expressed as follows:

$$\varepsilon_I(t) + \varepsilon_R(t) + \varepsilon_T(t) \quad (2)$$

Substituting Eq. 2 into Eq. 1, the two-wave method function for SHPB experimental data was obtained as follows (Yin et al., 2019; Lu et al., 2019):

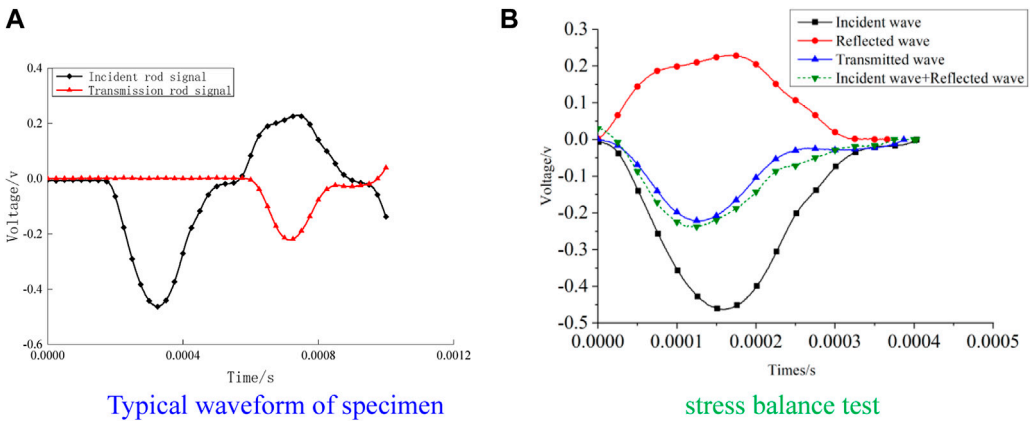

FIGURE 6
Typical waveform of specimen and stress balance test. **(A)** Typical waveform of specimen. **(B)** Stress balance test.

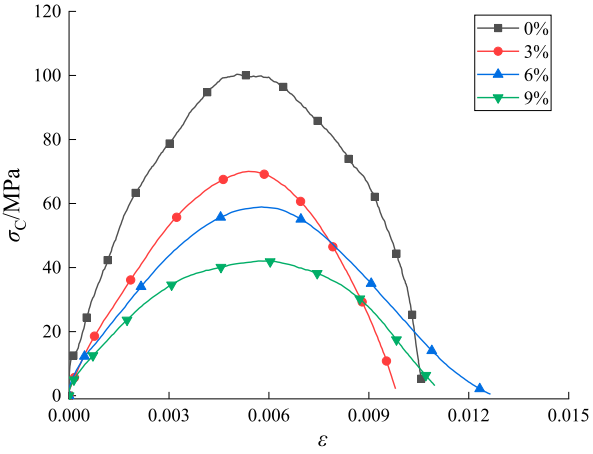

FIGURE 7
Stress–strain curve of concrete specimens under different sulfate concentrations and high strain rates.

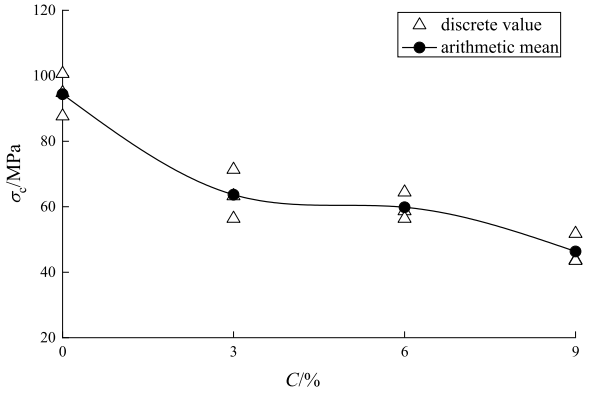

FIGURE 8
Variation curve of dynamic peak strength σ_C of specimens under high strain rate with the sulfate concentration C.

$$\begin{cases} \varepsilon(t) = -2\dfrac{C_0}{L_s}\displaystyle\int_0^t \varepsilon_R(t)dt \\ \dot{\varepsilon}(t) = -2\dfrac{C_0}{L_s}\varepsilon_R(t) \\ \sigma(t) = \dfrac{A_0}{A_s}E_0\varepsilon_T(t) \end{cases} \tag{3}$$

3.2 Effect of corrosive solution concentration on the stress-strain curve of the specimen

Equations 1–3 are used to process the original waveform curve shown in Figure 6, and the stress-strain curve of specimens after impact compression under sulfate attack of different concentrations is obtained, as shown in Figure 7.

As shown in Figure 7, the stress-strain curve of concrete specimens under different concentrations of sulfate attack is almost similar, which can be divided into the approximate linear-elastic stage, microcrack evolution and unstable propagation stage, and strain softening stage. However, there are certain differences in the basic characteristics of each stage. Specifically, the peak stress of the specimen decreases significantly with the increase of the concentration of the erosion solution; The slope of the stress-strain curve in the approximate linear-elastic stage decreases with the increase of the concentration of the erosion solution.

3.3 Effect of corrosive solution concentration on mechanical properties of the concrete specimen

According to the stress-strain curve of concrete specimens under the sulfate attack and high strain rate, the dynamic mechanical parameters of specimens under different sulfate concentrations can be obtained, as shown in Table 4.

Figure 8 shows the variation curve of dynamic peak strength of specimens under high strain rate with the sulfate concentration. As shown in Figure 8, the change in sulfate concentration has a significant impact on the dynamic peak strength of concrete specimens. The peak strength of concrete subjected to sulfate attack has decreased compared to the strength of non-corroded specimens. Specifically, as the sulfate concentration increases, the peak strength of concrete shows a downward trend. The specific process of change is as follows: 1) When the concentration of the erosion solution increases from 0.0% to 3.0%, the compressive strength of the sample decreases significantly, from 94.36 MPa to 63.67MPa, with a decrease of 32.53%; 2) When the concentration of the eroded solution C=6.0%, the compressive strength of the sample decreases to 59.83MPa, which is about 36.60% lower than that of the non-eroded sample; 3) When the concentration of the eroded solution C=9.0%, the compressive strength of the sample decreases to 46.34MPa, which is about 50.90% lower than that of the non-eroded sample. The changes in dynamic peak strength of concrete specimens with the sulfate concentration indicate that an increase in sulfate concentration reduces the impact resistance of concrete.

As shown in Figure 9, the change in sulfate concentration has a significant impact on the dynamic elastic modulus of concrete. The elastic modulus of concrete under the sulfate attack has decreased compared to the non-corroded specimen. Specifically, as the sulfate concentration increases, the dynamic elastic modulus of concrete shows a downward trend. The change process is as follows: 1) When the concentration of the erosion solution increases from 0.0% to 3.0%, the elastic modulus of the sample decreases from 35.10 GPa to 27.52 GPa, with a decrease of 21.58%; 2) When C=6.0%, the elastic modulus of the sample decreases to 17.65GPa, which is about 49.70% lower than that of the non-eroded sample; 3) When C=9.0%, the elastic modulus of the sample decreases to 15.85GPa, which is about 54.84% lower than that of the non-eroded sample. The changes in the dynamic elastic modulus of concrete with the sulfate concentration indicate that an increase in sulfate concentration reduces the resistance of concrete to elastic deformation.

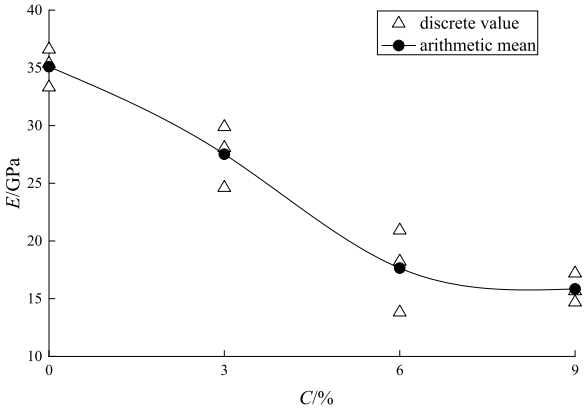

FIGURE 9
Variation curve of the elastic modulus *E* of the specimen under high strain rate with the corrosive solution concentration *C*.

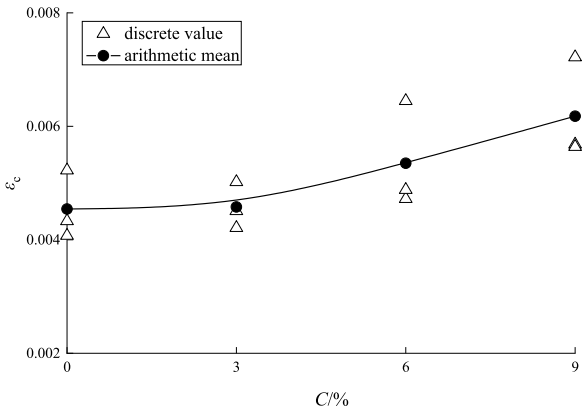

FIGURE 10
The variation curve of peak strain ε_c of the specimen with the concentration C of corrosive solution under the high strain rate.

As shown in Figure 10, the sulfate concentration significantly affects the dynamic peak strain of concrete. As the sulfate concentration increases, the dynamic peak strain of concrete shows an upward trend. The specific change process is as follows: 1) When the concentration of the erosion solution increases from 0.0% to 3.0%, the peak strain of the sample does not change much, increasing from 0.004543 to 0.004579; 2) When *C*=6.0%, the peak strain of the sample increases to 0.005350, which is about 17.76% higher than that of the non eroded sample; 3) When *C*=9.0%, the peak strain of the sample increases to 0.006179, which is approximately 36.02% higher than that of the non-eroded sample. The changes in dynamic peak strain and sulfate concentration of concrete indicate that an increase in sulfate concentration reduces the deformation resistance of concrete.

The alterations in the mechanical characteristics of concrete primarily arise from two factors. On the one hand, the increase in sulfate concentration leads to a decrease in the content of $Ca(OH)_2$, which is one of the components used in the later production of calcium carbonate in concrete. The decrease in $Ca(OH)_2$ content

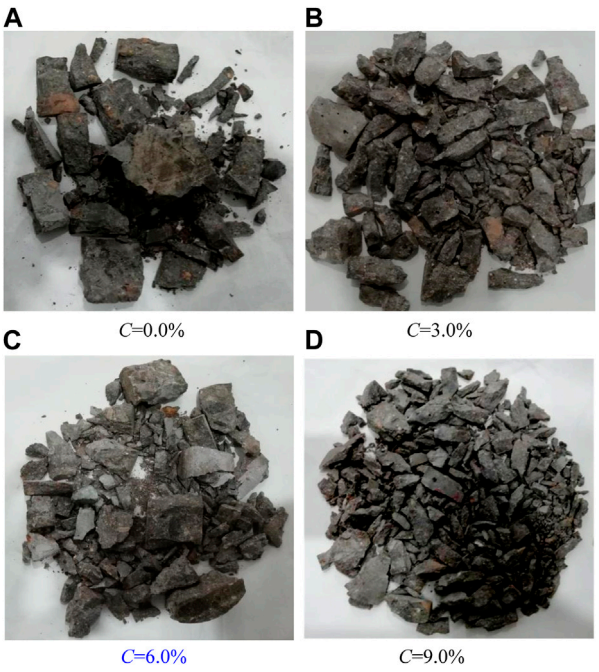

FIGURE 11
Failure morphology of sulfate-corroded specimens under different concentrations and high strain rates. **(A)** C = 0.0%. **(B)** C = 3.0%. **(C)** C = 6.0%. **(D)** C = 9.0%.

further leads to a decrease in the generated calcium carbonate content, thereby reducing the interfacial force of internal substances (Santhanam and Otieno, 2016). As a consequence, the compressive and deformation resistance of concrete is reduced under impact conditions. On the other hand, as the concentration of sulfate ions increases, the number of AFt gradually increases, leading to the expansion in the internal pores inside the concrete. Consequently, the development and propagation of cracks are promoted, which further reduces the integrity and stability of the concrete. Therefore, as the sulfate concentration increases, the dynamic peak strain of concrete increases, while the dynamic peak strength and elastic modulus of concrete decrease.

3.4 Effect of corrosive solution concentration on macroscopic failure characteristics of specimens

Figure 11 shows the failure morphology of specimens under high strain rates and the sulfate attack at different concentrations. As illustrated in Figure 10, as the concentration of the corrosive solution increases, the fragmentation degree of the specimen gradually increases, and the particle size of the specimen fragments decreases. Under the impact load, the damage degree of the specimen subjected to sulfate attack is higher than that of the specimen free from sulfate attack. When the non-corroded specimen still retains a portion of the main body, the sulfate-corroded specimen has broken into a pile of residue.

Due to the sulfate intrusion, chemical reaction with the internal materials of concrete occurs to generate ettringite and other reaction products. With the accumulation of reaction products, the surrounding materials are squeezed to a certain extent, resulting in radial cracks from the inside out. Consequently, the integrity and stability of concrete is reduced. As the concentration of the corrosive solution increases, more and more SO_4^{2-} enters the interior of the specimen, leading to an increase in erosion products. In particular, a large number of AFt crystals is generated at the interface between cement and aggregate, and the AFt crystals in the pores of concrete specimens are extruded. As a result, the inside of the specimen gradually loosens, expansion cracks increase (Yin et al., 2019), and the fragmentation degree of concrete increases. Under a similar strain rate, the higher the sulfate concentration, the more severe the damage of concrete fragments.

3.5 Effect of corrosive solution concentration on particle size distribution characteristics of specimens

In order to quantify the impact of sulfate concentration on the degree of concrete damage, concrete fragments of different particle sizes was screened and the proportion was calculated under different sulfate concentrations.

The specific process is as follows: first, the concrete fragments under different sulfate concentrations was screened by a grading screen, and the fragments was divided into eight groups of particle sizes: 74-50mm, 50-30mm, 30-20mm, 20-10mm, 10-5mm, 5-3mm, 3-1mm, 1-0mm, with particle size codes i being 1–8; Then, the mass of fragmentation of each level was weighed by an electronic scale with an accuracy of 0.01 g. At the same time, the mass percentage of fragmentation in the overall mass for each particle size range was calculated:

$$n_i = m_i/m \tag{4}$$

In the formula, i is the number of grading sieve grades (i=1,2. 8), n_i is the mass proportion of the fragments under this particle size, m_i is the mass of the fragments under this particle size, and m is the total mass of the concrete sample.

The average particle size of concrete fragments under different sulfate concentrations was calculated using the following equation:

$$\eta = \sum_{i=1}^{8} n_i r_i \tag{5}$$

In the formula, η is the average particle size of concrete fragments, r_i is the average particle size of each grading group.

Figure 12 shows the size distribution of concrete fragments under different concentrations of sulfate attack. As shown in Figure 12, the change in sulfate concentration has a significant impact on the distribution of particle size of concrete fragments under the effect of uniaxial impact compression. Average particle size shows a decrease trend with the increase of sulfate concentration. The specific process of change is as follows: 1) When the concentration of the erosion solution increases from 0.0% to 3.0%, the average particle size of the sample decreases from 24.02 mm to 22.57mm, with a decrease of 6.04%; 2) When the concentration of the eroded solution C=6.0%, the average particle size of the sample decreases to 21.48mm, which is about 10.57% lower than that of the non-eroded sample; 3) When the concentration of the eroded solution C=9.0%, the average particle size of the sample decreases to 18.58mm, which is about 22.65% lower than that of the non-eroded sample. Besides, the mass percentage of larger particle sizes (greater than 30 mm) shows a trend of first increasing and then decreasing with the increase of sulfate concentration, while the mass percentage of smaller particle sizes (less than 30 mm) shows a trend of first decreasing and then increasing with the increase of sulfate concentration. The size distribution of concrete fragments varies with the concentration of sulfate, indicating that sulfate has a significant impact on the impact resistance of concrete.

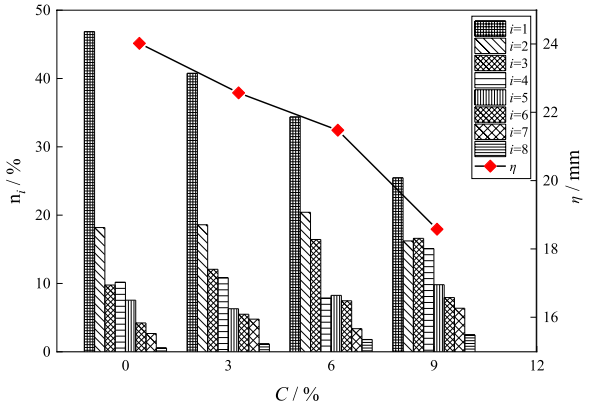

FIGURE 12
Particle size distribution of concrete fragments under different concentrations of sulfate.

4 Effect of sulfate concentration on energy change of concrete under the high strain rate

4.1 Energy calculation principle of concrete under dynamic load

According to the test principle, the energy dissipation of concrete specimens in the process of impact loading can be calculated through the input and output of energy in the pressure rod system. According to the elastic wave theory, the calculation function for the incident energy W_I J), reflected energy W_R J), and transmitted energy W_T J), in the SHPB experimental system are as follows (Yin et al., 2019; Lu et al., 2019):

$$\begin{cases} W_I = \dfrac{A_0 C_0}{E_0}\int_0^t \sigma_I^2(t)dt = A_0 C_0 E_0 \int_0^t \varepsilon_I^2(t)dt \\ W_R = \dfrac{A_0 C_0}{E_0}\int_0^t \sigma_R^2(t)dt = A_0 C_0 E_0 \int_0^t \varepsilon_R^2(t)dt \\ W_T = \dfrac{A_0 C_0}{E_0}\int_0^t \sigma_T^2(t)dt = A_0 C_0 E_0 \int_0^t \varepsilon_T^2(t)dt \end{cases} \tag{6}$$

Where W_I, W_R and W_T represent the incident energy, reflected energy, and transmitted energy in the system; A_0, C_0 and E_0 represent the cross-sectional area, (m^2), wave velocity (m/s), and

TABLE 5 Energy calculation results of uniaxial impact compression of concrete under different sulfate concentrations.

C/%	Reflected energy W_R/J		Transmitted energy W_T/J		Dissipated energy W_L/J	
	Discrete value	Average	Discrete value	Average	Discrete value	Average
0	38.89	28.84	93.96	96.54	10.43	16.69
	23.4		92.09		19.16	
	24.22		103.58		20.48	
3	39.04	58.80	78.67	75.27	36.06	34.99
	40.30		69.74		38.37	
	42.07		77.39		30.55	
6	41.58	71.75	43.82	47.20	43.75	44.06
	40.76		42.08		47.20	
	47.90		55.69		41.23	
9	42.03	46.09	16.64	18.45	63.93	59.96
	43.06		17.03		78.46	
	53.17		21.67		37.5	

elastic modulus of the compression rod (Pa);σ_I, σ_R and σ_T represent the stress (Pa)generated by incident waves, reflected waves, and transmitted waves in the compression rod.

Since butter is applied on the end face of the specimen to reduce the frictional effect on the end face, the frictional energy between the specimen and the compression rod can be ignored. Therefore, in the SHPB experiment, the absorbed energy W_L can be expressed as (Yin et al., 2019; Lu et al., 2019):

$$W_L = W_I - (W_R + W_T) = A_0 C_0 E_0 \int_0^t \left\{ \varepsilon_I^2(t) - \left[\varepsilon_R^2(t) + \varepsilon_T^2(t) \right] \right\} dt \tag{7}$$

where W_L represents the absorbed energy (or dissipated energy) during specimen failure.

In the SHPB experiment, energy dissipation mainly includes the energy dissipation caused by specimen crack propagation (W_{LD}), fragment motion energy dissipation (W_{LV}), and other energy dissipation (W_{LS}) such as frictional energy consumption. However, W_{LV} and W_{LS} account for a small proportion of W_L, and over 95% of the energy is used for crack propagation in the specimen. Therefore, it can be roughly assumed that W_L=W_{Ld}.

4.2 Impact of sulfate concentration on various energy changes in concrete

By using Equations 6, (7), the energy of concrete under impact load can be obtained, and the calculation results are shown in Table 5.

Figure 13 shows the energy variation in concrete with different sulfate concentrations. It can be seen that as the concentration of sulfate increases, the reflected energy of concrete first increases and then decreases, the dissipated energy gradually increases, and the transmitted energy gradually decreases. When the sulfate concentration is 0%, the reflected energy of concrete is 28.84 J; As the sulfate concentration increases to 9%, the reflected energy of concrete is 46.09 J, increasing by 59.82%. When the sulfate concentration is 0%, the transmitted energy of concrete is 96.54 J; As the sulfate concentration increases to 9%, the transmitted energy of concrete is 18.45 J, decreasing by 80.89% compared to the sulfate concentration of 0%. When the sulfate concentration is 0%, the dissipated energy of concrete is 16.69 J; As the sulfate concentration increases to 9%, the dissipated energy of concrete is 59.96 J, decreasing by 259.28%.

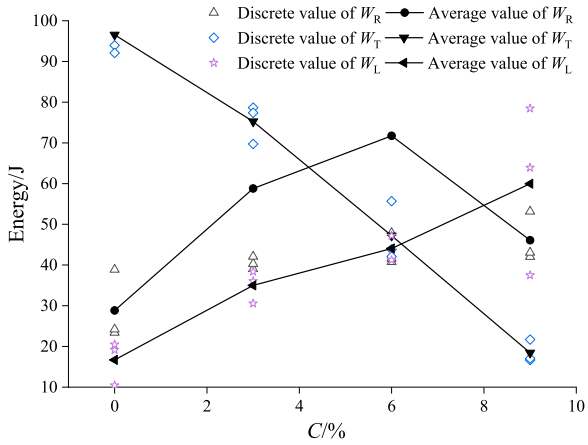

FIGURE 13
Energy variation in concrete at different sulfate concentrations.

To analyze the influence of sulfate concentration on energy variation in concrete under similar strain rates, the proportion of each energy in the total energy is analyzed. Figure 14 shows the variation of the percentage of each energy in the total energy of concrete with the concentration of sulfate. It can be seen that as the concentration of sulfate increases, the percentage of reflected energy and dissipated energy in the total energy gradually increases, while the

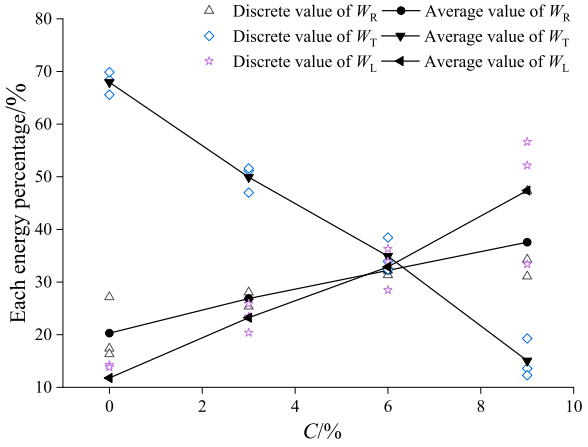

FIGURE 14
Variation curves of the percentage of each energy in total energy in concrete with sulfate concentration.

FIGURE 15
Scanning electron microscope.

percentage of transmitted energy in the total energy gradually decreases. When the sulfate concentration is 0%, the proportion of reflected energy in concrete is 20.29%; As the sulfate concentration increases to 9%, the proportion of reflected energy of concrete is 37.56%, increasing by 17.27%. When the sulfate concentration is 0%, the proportion of transmitted energy of concrete is 67.94%; As the sulfate concentration increases to 9%, the proportion of transmitted energy of concrete is 15.05%, decreasing by 52.89% compared to the sulfate concentration of 0%. When the sulfate concentration is 0%, the proportion of dissipated energy of concrete is 11.77%; As the sulfate concentration increases to 9%, the proportion of dissipated energy is 47.39%, increasing by 35.62% compared to the sulfate concentration of 0%.

The internal physical characteristics of concrete are changed after a sulfate attack, which is mainly due to the change of the cracked joints inside the concrete. According to the existing research (Wang et al., 2006; Cheng et al., 2020c; Cheng et al., 2021; Cheng et al., 2022; Song et al., 2022; Song et al., 2023), the free reflection stage and the transmission stage will occur when the stress wave propagates in the joint. In the free reflection stage, the gap is not closed, and the stress wave incident to the free boundary, produce only reflected waves and no transmitted waves. Under the action of stress wave, the particles on the interface move to the next interface, which makes the gap may close. Once the gap is fully closed, the energy will continue to propagate to the next interface, and so on, all the way to the transmission rod; Therefore, the joint opening can be well reflected by the reflected energy, transmitted energy and dissipated energy.

With the gradual increase of sulfate solution concentration, the proportion of reflected energy increases gradually. This can be explained as follows: the chemical reaction of some materials inside the concrete (such as calcium hydroxide)leads to the loss of the internal material volume and the formation of joint fissure; at the same time, the generated ettringite enlarges the joint fissure, leading to the gradual increase of the proportion of reflected energy and the gradual decrease of the proportion of transmitted energy during the propagation of stress waves under the same strain rate. The increase in the number of cracks, joints, and defect surfaces reduces the stability of concrete, leading to a decrease in its resistance to damage. As a result, more cracks, joints and defect surfaces are involved in the crack development and expansion under the uniaxial impact compression, the proportion of dissipated energy increases with the increase of sulfate concentration, and the energy absorption capacity of the sample is significantly improved contributing to the serious macroscopic damage to the concrete specimen.

5 Microstructure characteristics of concrete subjected to sulfate attack at high strain rate

5.1 Experimental equipment and methods

The VGEA3 scanning electron microscope test system of TESCAN Company of Czech Republic, which was introduced into the Civil structure laboratory of Xuzhou Institute of Technology, was adapted in this test, as shown in Figure 15.

At first, the damaged fragments of specimens subjected to sulfate attack at high strain rates were selected and made into cubes with a size of about 10×10×10mm, and then subjected to ultrasonic treatment in ethanol and then dried at 105 °C for 12 h. Subsequently, the specimen was pasted onto the specimen stable with latex for surface gilding, and the treated specimen was placed on the scanning electron microscope for microscopic observation.

5.2 Variation of concrete microstructure with corrosive solution concentration

To further observe the distribution of hydration and erosion products inside the specimen, SEM with a magnitude of

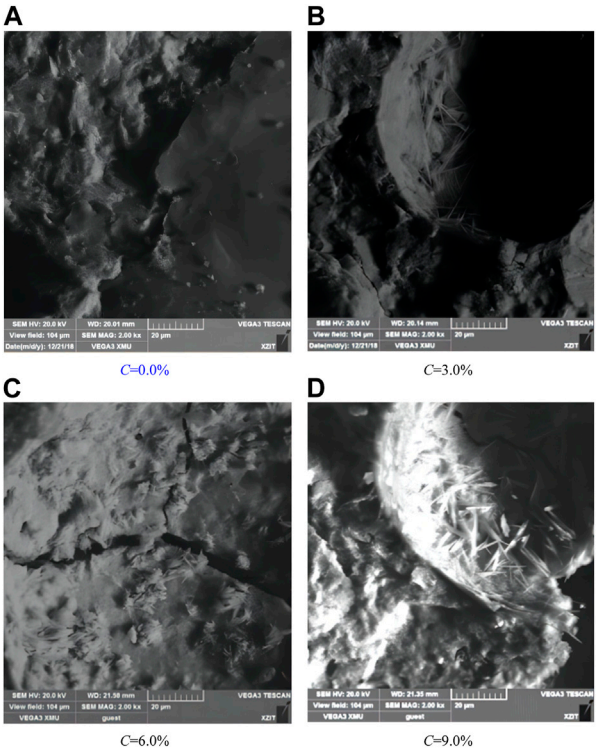

FIGURE 16
Distribution characteristics of internal hydration products and erosion products of concrete under sulfate attack. **(A)** C = 0.0%. **(B)** C = 3.0%. **(C)** C = 6.0%. **(D)** C = 9.0%.

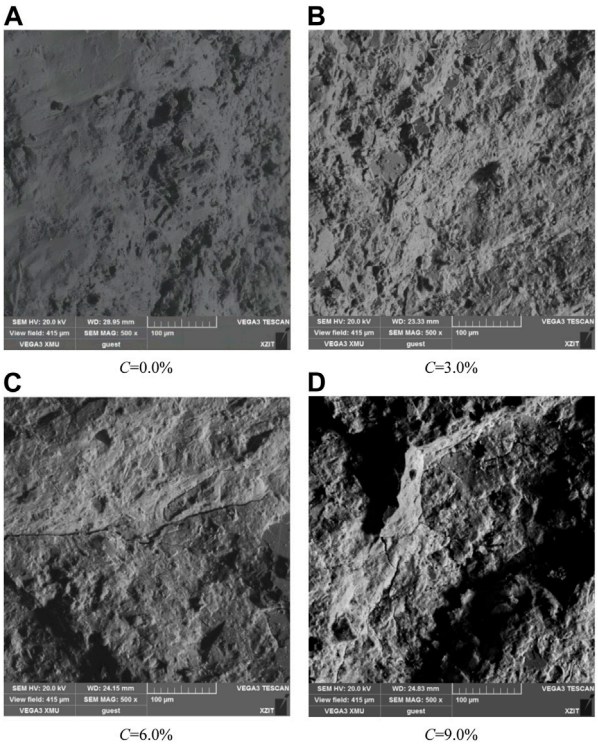

FIGURE 17
Variation characteristics of cracks in concrete under sulfate attack. **(A)** C = 0.0%. **(B)** C = 3.0%. **(C)** C = 6.0%. **(D)** C = 9.0%.

1000–2000 × was used to observe the selected area in the concrete specimen. Figure 16 shows the distribution characteristics of internal hydration products and erosion products of concrete under sulfate attack. It can be seen that a large number of $Ca(OH)_2$ crystals and acicular ettringite AFt can be found in the non-eroded specimen; As the concentration of the corrosive solution increases, the number of $Ca(OH)_2$ crystals decreases or even disappear upon visual observation, while the number of AFt crystals gradually increase. The erosion product AFt crystals are mainly distributed in the pores inside the specimen and the interface area of the cement aggregate, as shown in Figures 16B–D. This is due to the presence of large gaps and many pathways within the pores and interface regions of the specimen, facilitating easier transport of SO_4^{2-}. As a consequence, the number of erosion products sharply increases.

Figure 17 shows the characteristics of crack changes in concrete under sulfate attack. It can be seen that there are fewer microcracks in the non-eroded specimen, and as the concentration of the corrosive solution increases, the number of internal cracks in the specimen increase; The joint fissure in the non-corroded concrete specimens are scattered and have smaller sizes. As the sulfate concentration increases, the scattered distribution of the joint fissure gradually expands to a radial and network distribution state, and the size of the joint fissure is larger.

6 Conclusion

In this study, the uniaxial impact compression test of concrete specimens under sulfate attack was carried out, obtaining the correlation between sulfate erosion concentration, energy dissipation characteristics, and dynamic mechanical properties. The main conclusions are as follows:

1) XRD experiments indicate that with the increase of sulfate concentration, calcium hydroxide shows a downward trend as a whole, and AFt shows an upward trend as a whole.
2) As the concentration of sulfate increases, the dynamic peak strength and elastic modulus of concrete decrease, while the dynamic peak strain increases. The fragmentation degree of the concrete becomes more severe with the increase of sulfate concentration.
3) With the increase of sulfate concentration, the reflected energy of concrete first increases and then decreases, the dissipated energy gradually increases, and the transmitted energy gradually decreases; The proportion of reflected energy and dissipated energy gradually increases, while the proportion of transmitted energy gradually decreases.
4) SEM experiments indicate that as the concentration of the corrosive solution increases, the content of AFt gradually increases and the development of cracks became more obvious. Aft is concentrated in pores and at the interface between cement and aggregate.

Data availability statement

The original contributions presented in the study are included in the article/supplementary material, further inquiries can be directed to the corresponding author.

Author contributions

RL: Writing–original draft. LZ: Writing–review and editing. HL: Data curation, Writing–review and editing. BL: Writing–original draft.

Funding

The author(s) declare financial support was received for the research, authorship, and/or publication of this article. This work was supported by the National Science Foundation of China (52074240); Shandong Province Natural Science Foundation (ZR2021QD102).

Conflict of interest

The authors declare that the research was conducted in the absence of any commercial or financial relationships that could be construed as a potential conflict of interest.

Publisher's note

All claims expressed in this article are solely those of the authors and do not necessarily represent those of their affiliated organizations, or those of the publisher, the editors and the reviewers. Any product that may be evaluated in this article, or claim that may be made by its manufacturer, is not guaranteed or endorsed by the publisher.

References

Bai, M., Lu, Y., Zhang, Z., Cao, K., Cai, L., and Li, H. (2022). Relationship Between Microscopic Pore Structure and Strength of Cement-Based Materials with Low Water-Binder Ratio Under Sulfate Attack Environment. *Sci. Adv. Mater.* 14 (4), 725–735. doi:10.1166/SAM.2022.4254

CefisComi, N. C. (2014). Damage modelling in concrete subject to sulfate attack. *Frat. Integrita Strutt.* 8 (29), 222–229. doi:10.3221/IGF-ESIS.29.19

Chen, C., Huang, H., Yan, W., and Zhai, Y. (2008). Constitutive model of corroded concrete under uni-axial compression. *J. Huazhong Univ. Sci. Technol.* 36 (3), 38–39. doi:10.3901/JME.2008.05.160

Cheng, Y., Song, Z., Chang, X., and Wang, T. (2020a). Energy evolution principles of shock-wave in sandstone under unloading stress. *KSCE J. Civ. Eng.* 24, 2912–2922. doi:10.1007/s12205-020-1691-9

Cheng, Y., Song, Z., Jin, J., Wang, T., and Yang, T. (2020b). Waveform characterization and energy dissipation of stress wave in sandstone based on modified SHPB tests. *Geomechanics Eng.* 22 (2), 187. doi:10.12989/gae.2020.22.2.187

Cheng, Y., Song, Z. P., Jin, J. F., and Huang, J. H. (2020c). Continuous Cell Separation Using Microfluidic-Based Cell Retention Device with Alternative Boosted Flow. *J. Vib. Shock* 39 (8), 151–163. doi:10.1007/s12010-020-03288-9

Cheng, Y., Song, Z., Song, W., Li, S., Yang, T., and Zhang, Z. (2021). Strain performance and fracture response characteristics of hard rock under cyclic disturbance loading. *Geomechanics Eng.* 26 (6), 551–563. doi:10.12989/gae.2021.26.6.551

Cheng, Y., Song, Z., Yang, T., Han, J., Wang, B., and Zhang, Z. (2022). Investigating the aging damage evolution characteristics of layered hard sandstone using digital image correlation. *Constr. Build. Mater.* 353, 128838. doi:10.1016/j.conbuildmat.2022.128838

ChenLiuYu, Y. P. Z. (2020). Study on degradation of macro performances and micro structure of concrete attacked by sulfate under artificial simulated environment. *Constr. Build. Mater.* 260, 119951. doi:10.1016/j.conbuildmat.2020.119951

Demei, Y., Guan, B., He, R., Xiong, R., and Liu, Z. (2016). Sulfate attack of Portland cement concrete under dynamic flexural loading: A coupling function. *Constr. Build. Mater.* 115, 478–485. doi:10.1016/j.conbuildmat.2016.02.052

Feng, X., Huang, Z., Bi, Q. D., Liu, J., and Shuai, L. (2009). Study on the sulfate corrosion of concrete under the action of loading. *Key Eng. Mater.* 400/402, 175–180. doi:10.4028/www.scientific.net/KEM.400-402.175

Guo, J., Zhang, J., Yu, H., and Ma, H. (2023). Dynamic compressive behaviour of basic magnesium sulfate cement–coral aggregate concrete (BMSC–CAC) after exposure to elevated temperatures: experimental and analytical studies. *Constr. Build. Mater.* 382, 131336. doi:10.1016/J.CONBUILDMAT.2023.131336

Huangfu, X., Oiang, X. U., Hai yong, Y. U., and Wang, Q. (2004). *Application of marine high performance concrete to donghai bridge*. New York: World Bridge, 28–31. doi:10.3969/j.issn.1671-7767.2004.z1.008

Li, J., Xie, F., Zhao, G., and Li, L. (2020). Experimental and numerical investigation of cast-in-situ concrete under external sulfate attack and drying-wetting cycles. *Constr. Build. Mater.* 249, 118789. doi:10.1016/j.conbuildmat.2020.118789

LiHouHu, R. H. D., and Zou, Y. (2021). Effect of Concrete Micro-Mechanical Properties under the Coupled Corrosion of Sulfate and High Water Head. *Energies* 14 (16), 5039. doi:10.3390/en14165039

LiShiLi, Y. T. Y., Bai, W., and Lin, H. (2019). Damage of magnesium potassium phosphate cement under dry and wet cycles and sulfate attack. *Constr. Build. Mater.* 210, 111–117. doi:10.1016/j.conbuildmat.2019.03.213

Liu, P., Chen, Y., Yu, Z., Lu, Z., and Shi, W. (2020). Evolution of the dynamic properties of concrete in a sulfate environment. *Constr. Build. Mater.* 245, 118468. doi:10.1016/j.conbuildmat.2020.118468

Liu, T., Zou, D., Teng, J., and Yan, G. (2012). The influence of sulfate attack on the dynamic properties of concrete column. *Constr. Build. Mater.* 28 (1), 201–207. doi:10.1016/j.conbuildmat.2011.08.036

Lok, T. S., Li, X. B., Liu, D., and Zhao, P. J. (2001). Testing and response of large diameter brittle materials subjected to high strain rate. *J. Mater. Civ. Eng.* 14 (3), 262–269. doi:10.1061/(ASCE)0899-1561(2002)14:3(262)

Lu, A., Hu, S., Li, M., Duan, T., Li, B., and Chang, X. (2019). Impact of moisture content on the dynamic failure energy dissipation characteristics of sandstone. *Shock Vib.* 2019, 1–10. doi:10.1155/2019/6078342

Peng, L., Ying, C., Zhiwu, Y., and Zhaohui, L. (2019). Effect of sulfate solution concentration on the deterioration mechanism and physical properties of concrete. *Constr. Build. Mater.* 227 (10), 116641. doi:10.1016/j.conbuildmat.2019.08.022

QiangEnvelopeZw, F. Z. A., He, J., and Niu, D. (2022). Erosion behavior of ions in lining concrete incorporating fly ash and silica fume under the combined action of load and flowing groundwater containing composite salt. *Case Stud. Constr. Mater.* 17, e01659. doi:10.1016/j.cscm.2022.e01659

Santhanam, M., and Otieno, M. (2016). "Deterioration of concrete in themarine environment," in *Marine concrete structures*, 137–149. Cambridge, United Kingdom: Woodhead Publishing. doi:10.1016/B978-0-08-100081-6.00005-2

Song, Z., Cheng, Y., Zhang, Z., and Yang, T. t. (2023). Tunnelling performance prediction of cantilever boring machine in sedimentary hard-rock tunnel using deep belief network. *J. Mt. Sci.* 20 (7), 2029–2040. doi:10.1007/s11629-023-7931-y

Song, Z., Wang, T., Wang, J., Xiao, K., and Yang, T. (2022). Uniaxial compression mechanical properties and damage constitutive model of limestone under osmotic pressure. *Int. J. Damage Mech.* 31 (4), 557–581. doi:10.1177/10567895211045430

Tai, I., Cavalaro, S., Segura, I., de la Fuente, A., and Aguado, A. (2016). Simplified methodology to evaluate the external sulfate attack in concrete structures. *Mater. Des.* 89, 1147–1160. doi:10.1016/j.matdes.2015.10.084

Wang, W. H., Li, X. B., Zhou, Z. L., Zhang, Y. P., et al. (2006). Energy-transmitted rule of various stress waves across open joint. *J. Central South Univ. Sci. Technol.* 37 (2), 376–380. doi:10.1016/S1005-9040(06)60056-1

Wei, J., Cheng, B., Li, L., Long, W. J., and Khayat, K. H. (2023). Prediction of dynamic mechanical behaviors of coral concrete under different corrosive environments and its enhancement mechanism. *J. Build. Eng.* 63, 105507. doi:10.1016/j.jobe.2022.105507

Xia, W., Bai, E., Xu, J., and Liu, G. (2021). Experimental Study on the Strength and Deformation Characteristics of Concrete under True Triaxial Compression after Sulfate Attack. *Adv. Civ. Eng.* 2021, 1–15. doi:10.1155/2021/5548313

Xu, H., Chen, Z. Q., and Guo, X. Q. (2012). Physical and mechanical properties and influencing factors of high performance concrete under sulfate attack. *J. China Coal Soc.* 37 (2), 216–220. doi:10.13225/j.cnki.jccs.2012.02.007

Yao, A., Xu, J., and Xia, W. (2021). An Experimental Study on Mechanical Properties for the Static and Dynamic Compression of Concrete Eroded by Sulfate Solution. . *Mater.* 14 (18), 5387. doi:10.3390/ma14185387

Yao, M., and Li, J. (2018). Evolution of Mass and Strength of Concrete Cast-in-situ Piles Under Sulfate Medium Attack. *Tongji Daxue Xuebao/Journal Tongji Univ.* 46 (11), 1479–1485. doi:10.11908/j.issn.0253-374x.2018.11.002

YaoChen, J. J. (2022). Sensitivity analysis of the deterioration of concrete strength in marine environment to multiple corrosive ions. *Front. Struct. Civ. Eng.* 16 (2), 175–190. doi:10.1007/s11709-021-0791-z

Yin, G. J., Zuo, X. B., Sun, X. H., and Tang, Y. J. (2019). Macro-microscopically numerical analysis on expansion response of hardened cement paste under external sulfate attack. *Constr. Build. Mater.* 207, 600–615. doi:10.1016/j.conbuildmat.2019.02.159

Zhu, L., and Cao, D. (2008). Research on mechanics property of reinforced concrete bending members after corrosion of sulphate. *Shanxi Archit.* 34 (30), 7–8. doi:10.13719/j.cnki.cn14-1279/tu.2008.30.158

Zhu, L. (2009). *Study on mechanical properties of prestressed concrete flexural members corroded by sulfate*. Yangzhou: Yangzhou University. doi:10.7666/d.y1501265